

Fast simulation of soft x-ray near-edge spectra using a relativistic state-interaction approach: Application to closed-shell transition metal complexes

Sarah Pak,¹ Muhammed A. Dada,¹ Niranjan Govind,^{2,3} and Daniel R. Nascimento^{1, a)}

¹⁾ *Department of Chemistry, University of Memphis, Memphis, TN 38152, USA*

²⁾ *Physical and Computational Sciences Directorate, Pacific Northwest National Laboratory, Richland, WA 99352, USA*

³⁾ *Department of Chemistry, University of Washington, Seattle, WA 98195, USA*

Spectroscopic techniques based on core-level excitations provide powerful tools for probing molecular and electronic structures with high spatial resolution. However, accurately calculating spectral features at the L or M edges is challenging due to the significant influence of spin-orbit and multiplet effects. While scalar-relativistic effects can be incorporated at minimal computational cost, accounting for spin-orbit interactions requires more complex computational frameworks. In this work, we develop and apply the state-interaction approach, incorporating relativistic effects using the ZORA-Kohn-Sham Hamiltonian, to simulate near-edge soft X-ray absorption spectra for closed-shell transition metal complexes. The computed spin-orbit splittings closely match those obtained from more rigorous methods. This approach provides a practical and cost-effective alternative to more rigorous two-component methods, making it particularly valuable for large-scale calculations and applications such as resonant inelastic X-ray scattering simulations, where capturing a large number of excited states is essential.

I. INTRODUCTION

Spectroscopic techniques based on core-level excitations offer powerful tools for probing molecular and electronic structures with high spatial resolution and atomic specificity. Over the past decades, advancements in free-electron laser (FEL) technologies^{1–3} have made these techniques more widely accessible, enabling researchers to tackle a broad range of scientific questions^{4–12}.

Experiments at FEL facilities produce vast amounts of data that require thorough analysis and interpretation using theoretical models and computational simulations. However, advanced quantum chemistry methods, such as coupled-cluster theory, are computationally prohibitive for complex systems in realistic environments. Therefore, developing practical approaches that preserve essential physics while reducing computational costs—without compromising predictive accuracy—is crucial for advancing the field.

Density functional theory (DFT) based response approaches have proven highly effective in this context, offering a balance between accuracy and computational efficiency. For example, linear-response (LR) time-dependent density functional theory (TDDFT)^{13,14} and the Tamm-Dancoff Approximation (TDA) have been widely employed in the computation of X-ray spectra of molecules and solids^{15–17}, achieving remarkable success.

Accurate computation of spectral features at the L, M, or lower-energy edges, however, is significantly more complex due to the strong influence of spin-orbit (SO) coupling. In such cases, standard non-relativistic quantum chemistry approaches alone are insufficient to capture the

relevant physics. Instead, computations based on the real-time propagation of the Dirac-Kohn-Sham density matrix (RT-DKS)^{18,19}, 4-component (4c) Damped Response (DR) TDDFT²⁰, LR²¹ and real-time (RT)²² exact two-component relativistic (X2C) TDDFT, and relativistic two-component zeroth-order regular approximation (ZORA) TDDFT^{23–28} offer practical alternatives.

While scalar-relativistic (SR) effects can be seamlessly integrated into non-relativistic quantum chemistry codes with minimal impact on computational performance^{29–33}, SO interactions break spin symmetries, necessitating complex-valued spin-generalized frameworks that accommodate spin non-collinearity. The resulting algorithms can be up to $8\times$ more expensive than in the real-valued, spin-restricted case for ground-state DFT, and up to $32\times$ more expensive for LR-TDDFT.

In core-level spectroscopies, SO effects are significant even for relatively light elements. For example, the $L_{2,3}$ edge splittings of first-row transition metals (TMs) range from 5 to 10 eV — comparable to core-hole lifetime broadening — which causes overlap between the L_2 and L_3 features, making peak assignments very challenging. A similar trend is observed at the M and N edges of second and third-row TMs, respectively. While these shallow edges, accessible via soft X-rays, have historically been of little interest, current resonant-inelastic X-ray scattering (RIXS) experiments routinely probe them to gain deeper insights into the coupling between the core and valence excited states and the bonding characteristics of TM complexes^{12,34–40}.

Here, we employ a linear-response treatment of a ZORA-Kohn-Sham (ZKS) Hamiltonian based on the relativistic model potential of van Wüllen^{41,42}, to simulate the soft X-ray edge splittings of bare closed-shell transition metal cations and the near-edge X-ray absorption spectra of a series of closed-shell cyanometallates us-

^{a)} Electronic mail: daniel.nascimento@memphis.edu

ing the state-interaction ZKS approach with results that are comparable to state-of-the-art 4-component DKS and X2C methods. We also demonstrate that, in the present scenario, spin-orbit coupling effects can be efficiently introduced on top of a scalar-relativistic reference via the state-interaction approach. The spectra of a series of cyanometallates obtained with the present approach is shown to closely reproduce those generated by the fully variational X2C-LR-TDDFT method, at a significantly lower computational cost.

The paper is organized as follows: In Section II we describe the theory and working equations, the implementation is described in Section III, the computational details are given in Section IV, the results and discussion in Section V, and finally a conclusion in Section VI.

II. THEORY

A. Background

The ground-state ZORA-Kohn-Sham (ZKS) problem is defined as

$$\hat{h}^{\text{ZKS}}\varphi_i = \epsilon_i\varphi_i \quad (1)$$

with Hamiltonian given (in atomic units) by

$$\hat{h}^{\text{ZKS}} = \frac{\mathbf{p}^2}{2} + \mathbf{p} \left(\frac{\kappa - 1}{2} \right) \mathbf{p} + \frac{\kappa^2}{4c^2} \boldsymbol{\sigma} \cdot (\nabla v^{\text{KS}} \times \mathbf{p}) + v^{\text{KS}}. \quad (2)$$

Here, \mathbf{p} is the momentum operator, $\boldsymbol{\sigma}$ is a vector of Pauli spin matrices, and κ has the form

$$\kappa = \left[1 - \frac{v^{\text{KS}}}{2c^2} \right]^{-1}. \quad (3)$$

v^{KS} is the usual Kohn-Sham (KS) potential accounting for the external nuclear, Coulomb repulsion, and exchange-correlation potentials:

$$v^{\text{KS}}(\mathbf{r}) = - \sum_A \frac{Z_A}{|\mathbf{r} - \mathbf{R}_A|} + \int \frac{\rho(\mathbf{r}')}{|\mathbf{r} - \mathbf{r}'|} d\mathbf{r}' + \frac{\delta E_{\text{xc}}[\rho]}{\delta \rho(\mathbf{r})}. \quad (4)$$

The terms in the right-hand side of Eq. 2 can be easily identified as the classical kinetic energy, a scalar relativistic correction to the classical kinetic energy, the spin-orbit interaction, and the KS potential terms, respectively.

Direct application of the ZKS Hamiltonian in the form of Eq. 2, however, is known to be problematic as the dependence of the relativistic terms on the KS potential can lead to convergence and gauge-invariance issues⁴¹.

To bypass this problem and facilitate the evaluation of analytical geometry derivatives, van Wüllen⁴¹ proposed to replace the KS potential appearing in the relativistic terms (but not the last term in eq. 2) by an atom-based

effective potential of the form

$$v^{\text{eff}}(\mathbf{r}) = - \sum_A \frac{Z_A}{|\mathbf{r} - \mathbf{R}_A|} + \frac{\delta E_{\text{LDA}}[\tilde{\rho}]}{\delta \tilde{\rho}(\mathbf{r})} \quad (5)$$

$$+ \frac{2}{\sqrt{\pi}} \sum_{A,i} c_i^A \sqrt{\alpha_i^A} \times F_0(\alpha_i^A(\mathbf{r} - \mathbf{R}_A)^2),$$

where, F_0 denotes the Boys function, and c_i^A and α_i^A are the coefficients of the i th s -type Gaussian function centered on atom A , defining a model potential (provided in the SI). This model potential has the same components as the KS potential, however, the Coulomb and exchange-correlation terms are now evaluated with respect to a model density $\tilde{\rho}$ expressed as

$$\tilde{\rho}(\mathbf{r}) = \pi^{-3/2} \sum_{iA} c_i^A (\alpha_i^A)^{3/2} \exp(-\alpha_i^A |\mathbf{r} - \mathbf{R}_A|^2). \quad (6)$$

Note that in this effective potential, the exchange-correlation functional has been fixed as the local-density approximation (LDA) regardless of the exchange-correlation functional chosen for the SCF procedure. The obvious advantages of utilizing an effective potential of this form are the fact that it needs to be evaluated only once before the SCF cycle, and the ease to evaluate analytical derivatives, thus reducing the computational complexity of the overall procedure. In the present work, we adopt a slight modification by excluding the exchange-correlation term within the ZORA atomic model potential, while retaining it in the last term of Eq. 2. Previous work^{17,43-46} has shown that this term has negligible effect on ground and excited states.

Once the ZKS eigenpairs have been obtained self-consistently, we employ the scaled ZORA procedure of van Lenthe *et al.* to correct the *occupied* spinor energies up to first-order in the regular expansion⁴⁷:

$$\tilde{\epsilon}_i = \left(1 + \langle \varphi_i | \boldsymbol{\sigma} \cdot \mathbf{p} \frac{c^2}{(2c^2 - v^{\text{eff}})^2} \boldsymbol{\sigma} \cdot \mathbf{p} | \varphi_i \rangle \right)^{-1} \epsilon_i. \quad (7)$$

These energies are a better approximation to the 4-component DKS energies, thus providing a better starting point for our linear-response computations.

Finally, the linear-response TDDFT/TDA problem is solved employing the core-valence separation approach to obtain quasi-relativistic core-level excitation energies and oscillator strengths. Within the TDA,

$$AX = \Omega X \quad (8)$$

with

$$A_{iajb} = (\epsilon_a - \tilde{\epsilon}_i) \delta_{ij} \delta_{ab} + g_{iabj} - \alpha g_{ijba} + f_{iabj}^{\text{xc}}(\alpha). \quad (9)$$

Here, $f^{\text{xc}}(\alpha)$ denotes the scaled exchange-correlation kernel, where α is the hybrid parameter, and g_{pqrs} are electron repulsion integrals defined, respectively, as

$$f_{pqrs}^{\text{xc}}(\alpha) = \langle \varphi_p \varphi_r | \left[(1 - \alpha) \frac{\delta^2 E_{\text{x}}}{\delta \rho^2} + \frac{\delta^2 E_{\text{c}}}{\delta \rho^2} \right] | \varphi_q \varphi_s \rangle \quad (10)$$

and

$$g_{pqrs} = \langle \varphi_p \varphi_r | \frac{1}{|\mathbf{r} - \mathbf{r}'|} | \varphi_q \varphi_s \rangle. \quad (11)$$

Since the ZKS hamiltonian now includes spin-orbit interactions, spin is no longer a good quantum number and the TDDFT/TDA matrix will now contain spin-flip blocks with complex-valued entries. That is,

$$A = \begin{pmatrix} A_{\uparrow\uparrow\uparrow\uparrow} & A_{\uparrow\uparrow\uparrow\downarrow} & A_{\uparrow\uparrow\downarrow\uparrow} & A_{\uparrow\uparrow\downarrow\downarrow} \\ A_{\uparrow\downarrow\uparrow\uparrow} & A_{\uparrow\downarrow\uparrow\downarrow} & A_{\uparrow\downarrow\downarrow\uparrow} & A_{\uparrow\downarrow\downarrow\downarrow} \\ A_{\downarrow\uparrow\uparrow\uparrow} & A_{\downarrow\uparrow\uparrow\downarrow} & A_{\downarrow\uparrow\downarrow\uparrow} & A_{\downarrow\uparrow\downarrow\downarrow} \\ A_{\downarrow\downarrow\uparrow\uparrow} & A_{\downarrow\downarrow\uparrow\downarrow} & A_{\downarrow\downarrow\downarrow\uparrow} & A_{\downarrow\downarrow\downarrow\downarrow} \end{pmatrix}, \quad A \in \mathbb{C}. \quad (12)$$

This matrix has $8 \times$ as many elements as in the real-valued unrestricted case, where only the $A_{\uparrow\uparrow\uparrow\uparrow}$, $A_{\uparrow\uparrow\downarrow\downarrow}$, $A_{\downarrow\downarrow\uparrow\uparrow}$, and $A_{\downarrow\downarrow\downarrow\downarrow}$ blocks are non-zero, and $32 \times$ as many elements as in the real-valued restricted case, where only one block is needed. The construction of the spin-flip blocks strictly requires a non-collinear exchange-correlation functional, which we do not consider in this work.

Here, we consider two approximations where A is constructed with and without $f^{\text{xc}}(\alpha)$, while using a standard collinear functional for the ground state orbitals. The latter stems from a recent study by some of the authors, which demonstrated that $f^{\text{xc}}(\alpha)$ has no significant effect in the calculation of core-level spectra in transition metal complexes.⁴⁸ This approximation resembles a *scaled* configuration interaction singles (CIS) approach performed with approximate ZKS spinors. We refer to these as ZKS/TDA and ZKS/SCIS, respectively. SO interactions are introduced by using a state-interaction approach described below.⁴⁹

B. State-Interaction Approach

The state-interaction approach allows us to couple a set of states $\{|I\rangle\}$ via an operator \hat{V} by direct diagonalization of the matrix representation of \hat{V} in the basis spanned by $\{|I\rangle\}$. In the present context, this set of states is a subset of the solutions to the full scalar-relativistic (SR) TDA equations obtained by removing the SO term in the ZKS Hamiltonian, and \hat{V} is the SO-coupling operator. That is, we obtain SO-coupled excitation energies Ξ and states Z , by solving

$$\mathcal{H}^{\text{SO}} Z = \Xi Z, \quad (13)$$

with

$$\mathcal{H}_{IJ}^{\text{SO}} = \Omega_I \delta_{IJ} + \langle I | \frac{\kappa^2}{4c^2} \boldsymbol{\sigma} \cdot (\nabla v^{\text{eff}} \times \mathbf{p}) | J \rangle, \quad (14)$$

where Ω_I and $|I\rangle$ are related to the solutions of the scalar-relativistic TDA problem as

$$A^{\text{SR}} X = \Omega X, \quad \text{and } |I\rangle = \sum_{ia} X_{ia}^I \hat{a}_a^\dagger \hat{a}_i |\Phi_0\rangle. \quad (15)$$

Here, $|\Phi_0\rangle$ represents the reference KS determinant and indices i and a span occupied and virtual orbitals, respectively.

An immediate advantage of the state-interaction approach is that the scalar relativistic states can be obtained taking full advantage of real and spin symmetries. Furthermore, since \mathcal{H}^{SO} is constructed from a subset of $\{|I\rangle\}$, its dimension is only a fraction of the dimension of A^{SR} , making Eq. 15 the most expensive part of the procedure. Altogether, the approach outlined above leads to reduction in the computational cost by factors of $8 \times$ and $32 \times$ for unrestricted and restricted SR references, respectively. We will refer to these approaches as SR-ZKS/SCIS+SO, when A^{SR} is constructed without $f^{\text{xc}}(\alpha)$, and SR-ZKS/TDA+SO when A^{SR} is constructed with a standard collinear $f^{\text{xc}}(\alpha)$.

III. IMPLEMENTATION

Solving Eq. 1 requires evaluation of the ZORA integrals. These integrals are not standard in electronic structure theory, but can be easily evaluated in an atomic orbital basis set, $\{\chi_\mu\}$, with knowledge of the basis functions gradient, $\nabla \chi_\mu$, and the effective potential, v^{eff} evaluated using a numerical grid.

The scalar-relativistic kinetic energy integral takes the form

$$T_{\mu\nu}^{\text{SR}} = \int \chi_\mu^\dagger(\mathbf{r}) \left[\frac{\mathbf{p}^2}{2} + \mathbf{p} \cdot \left(\frac{\kappa - 1}{2} \right) \mathbf{p} \right] \chi_\nu(\mathbf{r}) d\mathbf{r} \quad (16)$$

$$= \int \frac{c^2}{2c^2 - v^{\text{eff}}(\mathbf{r})} \nabla \chi_\mu^\dagger(\mathbf{r}) \cdot \nabla \chi_\nu(\mathbf{r}) d\mathbf{r} \quad (17)$$

while the SO integral is given by

$$H_{\mu\nu}^{\text{SO}} = \int \chi_\mu^\dagger(\mathbf{r}) \left[\frac{\kappa^2}{4c^2} \boldsymbol{\sigma} \cdot \nabla v^{\text{eff}} \times \mathbf{p} \right] \chi_\nu(\mathbf{r}) d\mathbf{r} \quad (18)$$

$$= \boldsymbol{\sigma} \cdot \int \frac{v^{\text{eff}}(\mathbf{r})}{4c^2 - 2v^{\text{eff}}(\mathbf{r})} \nabla \chi_\mu^\dagger(\mathbf{r}) \times \nabla \chi_\nu(\mathbf{r}) d\mathbf{r}. \quad (19)$$

Note that since the operator in Eq. 17 does not have a spin component, $T_{\mu\nu}^{\text{SR}}$ will have a block-diagonal structure, facilitating its incorporation into standard non-relativistic electronic structure codes.

For convenience, it is useful to separate the spin and spatial components of $H_{\mu\nu}^{\text{SO}}$ and label the components of

the integral in the right-hand side of Eq. 19 explicitly as

$$h_{\mu\nu}^x = \int \frac{v^{\text{eff}}(\mathbf{r})}{4c^2 - 2v^{\text{eff}}(\mathbf{r})} \left[\frac{\partial\chi_\mu^\dagger}{\partial y} \frac{\partial\chi_\nu}{\partial z} - \frac{\partial\chi_\mu^\dagger}{\partial z} \frac{\partial\chi_\nu}{\partial y} \right] d\mathbf{r} \quad (20)$$

$$h_{\mu\nu}^y = \int \frac{v^{\text{eff}}(\mathbf{r})}{4c^2 - 2v^{\text{eff}}(\mathbf{r})} \left[\frac{\partial\chi_\mu^\dagger}{\partial z} \frac{\partial\chi_\nu}{\partial x} - \frac{\partial\chi_\mu^\dagger}{\partial x} \frac{\partial\chi_\nu}{\partial z} \right] d\mathbf{r} \quad (21)$$

$$h_{\mu\nu}^z = \int \frac{v^{\text{eff}}(\mathbf{r})}{4c^2 - 2v^{\text{eff}}(\mathbf{r})} \left[\frac{\partial\chi_\mu^\dagger}{\partial x} \frac{\partial\chi_\nu}{\partial y} - \frac{\partial\chi_\mu^\dagger}{\partial y} \frac{\partial\chi_\nu}{\partial x} \right] d\mathbf{r}, \quad (22)$$

where the spatial dependence of the atomic orbitals is implied. Upon taking the dot product with $\boldsymbol{\sigma}$, H^{SO} assumes the final form

$$H^{\text{SO}} = \begin{pmatrix} h^z & h^x - ih^y \\ h^x + ih^y & -h^z \end{pmatrix}. \quad (23)$$

H^{SO} is complex-valued, and will lead to spin-mixing, imposing the need for a complex-valued generalized self-consistent-field procedure to solve Eq. 1. However, as discussed in Section II B, this need can be bypassed by employing the state-interaction approach, which provides significant savings, especially when dealing with closed-shell systems. For these systems, the A^{SR} matrix can be spin-adapted to yield singlet and restricted triplet components:

$$A_{\text{SR}}^{0,0} S = \Omega^{0,0} S \quad (24)$$

$$A_{\text{SR}}^{1,0} T = \Omega^{1,0} T, \quad (25)$$

where

$$A_{iajb}^{0,0} = (\epsilon_a - \tilde{\epsilon}_i) \delta_{ij} \delta_{ab} + 2g_{iabj} - \alpha g_{ijba} + f_{iajb}^{\text{xc}}(\alpha) \quad (26)$$

$$A_{iajb}^{1,0} = (\epsilon_a - \tilde{\epsilon}_i) \delta_{ij} \delta_{ab} - \alpha g_{ijba} + f_{iajb}^{\text{xc}}(\alpha). \quad (27)$$

The real-valued solution vectors are then used to construct a 2-component complex spin basis, $\{|S, M_S\rangle\}$, in which the spin-orbit Hamiltonian will be evaluated:

$$|0, 0\rangle = \frac{1}{\sqrt{2}} \begin{pmatrix} S \\ S \end{pmatrix} \quad \text{and} \quad |1, 0\rangle = \frac{1}{\sqrt{2}} \begin{pmatrix} T \\ -T \end{pmatrix}. \quad (28)$$

The remaining triplet basis are obtained, without additional computation, through the action of raising and lowering spin operators on $|1, 0\rangle$:

$$|1, +1\rangle = \frac{1}{\sqrt{2}} (\sigma_x + i\sigma_y) |1, 0\rangle = \begin{pmatrix} 0 \\ T \end{pmatrix} \quad (29)$$

and

$$|1, -1\rangle = \frac{1}{\sqrt{2}} (\sigma_x - i\sigma_y) |1, 0\rangle = \begin{pmatrix} -T \\ 0 \end{pmatrix} \quad (30)$$

The block-structure of the spin-orbit Hamiltonian in the basis spanned by $|S, M_S\rangle = |0, 0\rangle \otimes |1, -1\rangle \otimes |1, 0\rangle \otimes |1, +1\rangle$ is then given by

$$\mathcal{H}_{\text{SO}} = \begin{pmatrix} \Omega^{0,0} & \frac{\sqrt{2}}{2} h_{\text{ST}}^{+1} & h_{\text{ST}}^0 & -\frac{\sqrt{2}}{2} h_{\text{ST}}^{-1} \\ \frac{\sqrt{2}}{2} h_{\text{TS}}^{-1} & \Omega^{1,0} + h_{\text{TT}}^0 & -\frac{\sqrt{2}}{2} h_{\text{TT}}^{-1} & 0 \\ h_{\text{TS}}^0 & -\frac{\sqrt{2}}{2} h_{\text{TT}}^{+1} & \Omega^{1,0} & -\frac{\sqrt{2}}{2} h_{\text{TT}}^{-1} \\ -\frac{\sqrt{2}}{2} h_{\text{TS}}^{+1} & 0 & -\frac{\sqrt{2}}{2} h_{\text{TT}}^{+1} & \Omega^{1,0} - h_{\text{TT}}^0 \end{pmatrix} \quad (31)$$

with

$$[h_{\text{ST}}^\xi]_{IJ} = \sum_{ia} S_{ia}^I \sum_{jb} (h_{ab}^\xi \delta_{ij} - h_{ji}^\xi \delta_{ab}) T_{jb}^J \quad (32)$$

$$[h_{\text{TS}}^\xi]_{IJ} = \sum_{ia} T_{ia}^I \sum_{jb} (h_{ab}^\xi \delta_{ij} - h_{ji}^\xi \delta_{ab}) S_{jb}^J \quad (33)$$

$$[h_{\text{TT}}^\xi]_{IJ} = \sum_{ia} T_{ia}^I \sum_{j,b} (h_{ab}^\xi \delta_{ij} + h_{ji}^\xi \delta_{ab}) T_{jb}^J. \quad (34)$$

Here, $\xi \in \{-1, 0, 1\}$ denote the components of the spin-orbit coupling matrix, given explicitly, in the canonical basis as

$$h_{pq}^0 = \sum_{\mu\nu} C_{\mu p} h_{\mu\nu}^z C_{\nu q} \quad (35)$$

$$h_{pq}^{+1} = \sum_{\mu\nu} C_{\mu p} (h_{\mu\nu}^x + ih_{\mu\nu}^y) C_{\nu q} \quad (36)$$

$$h_{pq}^{-1} = \sum_{\mu\nu} C_{\mu p} (h_{\mu\nu}^x - ih_{\mu\nu}^y) C_{\nu q}. \quad (37)$$

Finally, \mathcal{H}_{SO} can be diagonalized and the solution vectors, Z , can be used to evaluate transition dipole moments as

$$\boldsymbol{\mu}^n = \sqrt{2} \sum_{ia} \boldsymbol{\mu}_{ia} \sum_I S_{ia}^I Z_I^n, \quad (38)$$

where I and n denote uncoupled and coupled states, respectively.

IV. COMPUTATIONAL DETAILS

Geometries were optimized in the gas phase using the NWChem software package^{50,51}, and employed the PBE0^{52,53} exchange-correlation functional paired with the 6-31G*⁵⁴⁻⁵⁶ basis set for C and N, and the Sapporo-DKH3-DZP-2020-diffuse⁵⁷ basis set for the metal center. Scalar relativistic effects were taken into account by means of the SR-ZORA correction as implemented in NWChem⁴⁶, and point-group symmetry was enforced to speed-up optimizations. The resulting optimal geometric parameters are shown in Table I.

Excited-state calculations were performed employing the PBE0 exchange-correlation functional and the Dyall-v2z^{58,59} primitive basis set. The SR-ZKS/SCIS+SO, SR-ZKS/TDA+SO, and the fully 2-component SO-ZKS/SCIS methods were implemented as an *in-house*

Point Group	Complex	$r(M - C)$	$r(M - N)$
O_h	$[\text{Cr}(\text{CN})_6]^{6-}$	2.08	3.29
	$[\text{Mo}(\text{CN})_6]^{6-}$	2.13	3.24
	$[\text{W}(\text{CN})_6]^{6-}$	2.19	3.41
	$[\text{Fe}(\text{CN})_6]^{4-}$	1.97	3.15
	$[\text{Ru}(\text{CN})_6]^{4-}$	2.06	3.25
	$[\text{Os}(\text{CN})_6]^{4-}$	2.03	3.22
D_{2h}	$[\text{Cu}(\text{CN})_2]^-$	1.80	2.97
	$[\text{Ag}(\text{CN})_2]^-$	1.83	3.28
	$[\text{Au}(\text{CN})_2]^-$	1.80	3.24

TABLE I. Optimized geometrical parameters for the cyanometallates relevant to the present work. Atomic separations are shown in Å.

python code interfaced with the PySCF⁶⁰ quantum chemistry package, while reference DKS and X2C calculations were performed using the ReSpect code⁶¹.

V. RESULTS AND DISCUSSION

A. Bare Transition Metal Cations

In order to understand how well the modified ZORA effective potential described earlier is able to reproduce the Dirac–Kohn–Sham (DKS) Hamiltonian, we begin by calculating the SO splittings in the ZKS eigenvalues of a series of bare transition metal cations (Figure 1). Here, we focus on core-level orbitals with SO splittings between 2 and 40 eV. These are generally orbitals with principal quantum number $(N - 2)$, with N corresponding to the period in which the atom appears in the periodic table.

As shown in Figure 1, the SO splittings computed with the atomic-mean-field exact 2-component method (amfX2C) of Konecny *et al.*⁶² and the effective potential ZKS Hamiltonians, are essentially identical to the ones obtained with the more computationally expensive DKS Hamiltonian. The only Hamiltonian to perform poorly was the 1-electron X2C (1eX2C) Hamiltonian⁶², where relativistic 2-electron contributions are completely neglected. These results highlight the importance of accounting for two-electron relativistic corrections, even if it is done by means of an effective potential.

To better quantify the error in the SO splittings, we show the difference between the SO splitting obtained with the amfX2C, 1eX2C, and ZKS methods against those obtained with the reference DKS method in Figure 2. As one can observe, the error tends to increase monotonically across a period, but decreases across a group, with the largest absolute error for the ZKS method being 0.37 eV ($\approx 1\%$) for the Cd^{12+} 3p orbitals. The average (signed) error for ZKS across a period was evaluated to

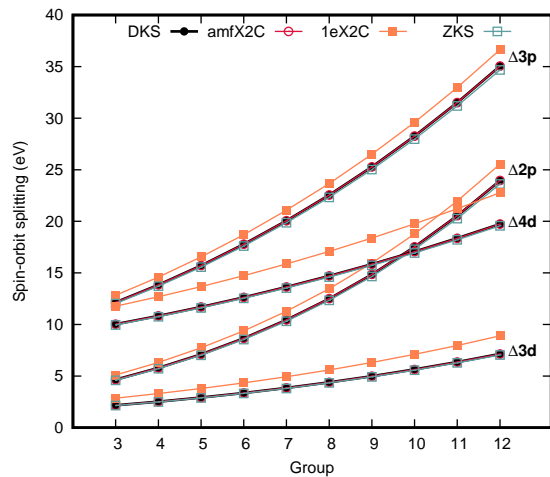


FIG. 1. SO splittings in the Kohn–Sham orbital energies for a series of bare, d^0 transition metal cations, computed with different relativistic Hamiltonians. Here, $\Delta 2p$, $\Delta 3p/3d$, and $\Delta 4d$, are computed for atoms in the 4th, 5th, and 6th periods of the periodic table, respectively.

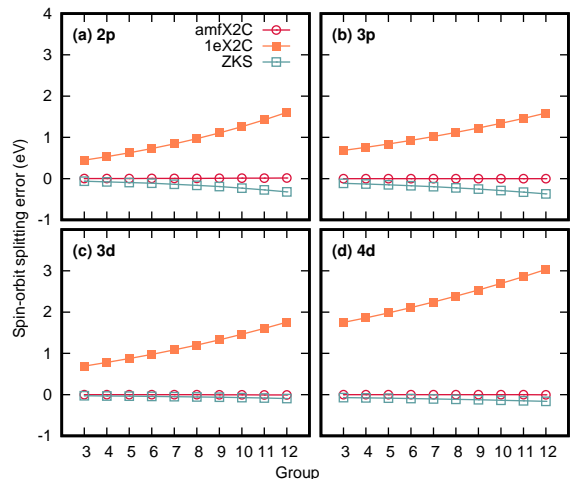


FIG. 2. Error in the SO splittings in the Kohn–Sham orbital energies for a series of bare, d^0 transition metal cations, computed with different relativistic Hamiltonians.

be -0.17, -0.22, -0.06, and -0.11 eV, for the 2p, 3p, 3d, and 4d orbitals, respectively. In contrast, the errors for 1eX2C method increase both across periods and groups, with the largest error reaching 3.04 eV ($>15\%$) for the Hg^{12+} 4d orbitals. For 1eX2C, the average errors were 0.95 (2p), 1.10 (3p), 1.18 (3d), and 2.35 eV (4d). The SO splittings for each cation calculated with different Hamiltonians are presented in Table II.

Next, we analyze how the choice of relativistic approximation affects the spectral near-edge splittings. In Figure 3, we report the splittings between excited states with dominant $2p_{3/2} \rightarrow 3d_{5/2}$ and $2p_{1/2} \rightarrow 3d_{3/2}$ character ($\Delta L_{2,3}$) for 4th-period cations, between excited states with dominant $3p_{3/2} \rightarrow 4d_{5/2}$ and $3p_{1/2} \rightarrow 4d_{3/2}$

$\Delta 2p$	Sc ³⁺	Ti ⁴⁺	V ⁵⁺	Cr ⁶⁺	Mn ⁷⁺	Fe ⁸⁺	Co ⁹⁺	Ni ¹⁰⁺	Cu ¹¹⁺	Zn ¹²⁺	MSD	RMSD
DKS	4.66	5.79	7.11	8.66	10.44	12.50	14.85	17.52	20.54	23.95		
amfX2C	4.66	5.79	7.11	8.66	10.45	12.51	14.86	17.53	20.55	23.96	0.01	0.00
1eX2C	5.11	6.32	7.74	9.38	11.29	13.47	15.96	18.78	21.97	25.55	0.95	0.32
ZKS	4.59	5.71	7.02	8.54	10.31	12.34	14.65	17.29	20.27	23.62	-0.17	0.06
$\Delta 3p$	Y ³⁺	Zr ⁴⁺	Nb ⁵⁺	Mo ⁶⁺	Tc ⁷⁺	Ru ⁸⁺	Rh ⁹⁺	Pd ¹⁰⁺	Ag ¹¹⁺	Cd ¹²⁺	MSD	RMSD
DKS	12.14	13.84	15.71	17.78	20.05	22.55	25.28	28.26	31.51	35.05		
amfX2C	12.14	13.84	15.71	17.78	20.05	22.55	25.28	28.26	31.51	35.04	-0.00	0.00
1eX2C	12.83	14.60	16.55	18.71	21.07	23.67	26.51	29.60	32.97	36.63	1.10	0.36
ZKS	12.03	13.71	15.56	17.61	19.86	22.33	25.03	27.97	31.18	34.68	-0.22	0.07
$\Delta 3d$	Y ³⁺	Zr ⁴⁺	Nb ⁵⁺	Mo ⁶⁺	Tc ⁷⁺	Ru ⁸⁺	Rh ⁹⁺	Pd ¹⁰⁺	Ag ¹¹⁺	Cd ¹²⁺	MSD	RMSD
DKS	2.17	2.52	2.92	3.36	3.85	4.39	4.99	5.64	6.36	7.14		
amfX2C	2.17	2.52	2.92	3.36	3.85	4.39	4.99	5.64	6.35	7.13	-0.00	0.00
1eX2C	2.86	3.30	3.79	4.34	4.94	5.60	6.32	7.11	7.97	8.90	1.18	1.18
ZKS	2.14	2.49	2.88	3.32	3.80	4.34	4.93	5.57	6.28	7.05	-0.06	0.02
$\Delta 4d$	Lu ³⁺	Hf ⁴⁺	Ta ⁵⁺	W ⁶⁺	Re ⁷⁺	Os ⁸⁺	Ir ⁹⁺	Pt ¹⁰⁺	Au ¹¹⁺	Hg ¹²⁺	MSD	RMSD
DKS	10.02	10.83	11.69	12.63	13.63	14.70	15.85	17.07	18.36	19.73		
amfX2C	10.02	10.83	11.69	12.63	13.63	14.70	15.85	17.06	18.36	19.73	-0.00	0.00
1eX2C	11.77	12.69	13.68	14.74	15.88	17.09	18.38	19.76	21.22	22.77	2.35	0.75
ZKS	9.95	10.75	11.61	12.54	13.53	14.59	15.72	16.93	18.21	19.57	-0.11	0.04

TABLE II. SO splittings, mean signed deviation (MSD), and root mean squared deviation (RMSD) in the Kohn–Sham orbital energies for a series of bare, d⁰ transition metal cations, computed with different relativistic Hamiltonians.

($\Delta M_{2,3}$), and $3d_{3/2} \rightarrow 5p_{1/2}$ and $3d_{1/2} \rightarrow 5p_{3/2}$ character ($\Delta M_{4,5}$) for 5th-period cations, and between excited states with dominant $4d_{3/2} \rightarrow 6p_{1/2}$ and $4d_{5/2} \rightarrow 6p_{3/2}$ character ($\Delta N_{4,5}$) for 6th-period cations. These excitations correspond to the dominant features in the soft X-ray absorption spectra. The excited-state energies are calculated using both the spinor-based approach, where the ground-state ZKS equations are solved with variational inclusion of scalar relativistic *and* spin-orbit effects, followed by a linear-response calculation, and the state-interaction approach as outlined earlier.

When comparing the spinor-based approaches, amfX2C/TDA reproduced the DKS/TDA results almost exactly, followed by the SO-ZKS/SCIS approach, which yields equally good results for the $L_{2,3}$, $M_{2,3}$, and $M_{4,5}$ splittings. For the $N_{4,5}$ splittings, the SO-ZKS/SCIS approach is indistinguishable from the reference (DKS/TDA) up to Fe⁸⁺, but deviations from the reference become pronounced beyond this point, reaching an error of almost 1 eV for Hg¹²⁺. One could think that this error is a manifestation of the scaled CIS approach for the excited states, but we demonstrate below that this is not the case. The performance of the 1eX2C/TDA method is overall poor, as expected given the large errors in the single-particle energies

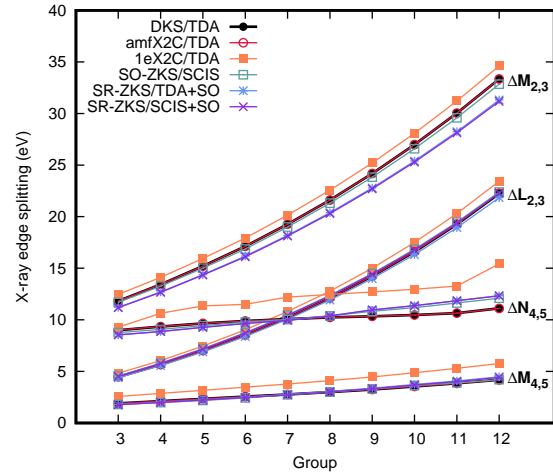


FIG. 3. X-ray near-edge splittings due to spin-orbit coupling for a series of bare, d⁰ transition metal cations, computed with different relativistic Hamiltonians and approximations. The splittings are calculated with respect to the spectral features with dominant $p_{3/2} \leftrightarrow d_{5/2}$ and $p_{1/2} \leftrightarrow d_{3/2}$ character.

shown in Figure 2, however, it is worth mentioning that

approaches able to reduce this error have been reported in the literature⁶³.

The two state-interaction approaches perform very similarly regardless of whether or not the exchange-correlation kernel is included in the construction of the TDA matrix. This observation is in corroboration with our previous study showing that the exchange-correlation kernel plays a negligible role in the calculation of core-level excited states⁴⁸, which also eliminates the removal of the exchange-correlation kernel in SO-ZKS/SCIS as a possible reason for the discrepancies in the $N_{4,5}$ splittings observed beyond Fe^{8+} . Furthermore, the fact that SR-ZKS/TDA+SO and SO-ZKS/SCIS predict very close $N_{4,5}$ splittings, implies that the variational inclusion of SO effects during ground state optimization does not significantly affect these states either, leaving the parametrization of the ZORA effective potential as the likely source of error. In contrast, the $M_{2,3}$ splittings, are significantly affected by the inclusion of SO effects during the ground state optimization. Finally, the $L_{2,3}$ and $M_{4,5}$ predicted by all ZKS approaches are in very close agreement with those calculated using the DKS/TDA method. Upon closer inspection, one can observe that in fact, the $L_{2,3}$ are very slightly affected by the neglect of the exchange-correlation kernel in the TDA matrix causing the SR-ZKS/TDA+SO splittings to be slightly underestimated with respect to the DKS/TDA ones (-0.2 eV in average), while the SR-ZKS/SCIS+SO and SO-ZKS/SCIS splittings are slightly overestimated (0.2 eV in average). These differences are better visualized in Figure 4, which reports the error in the edge splittings with respect to the DKS/TDA reference. The edge splittings for individual cations and corresponding error analysis are provided in Table III.

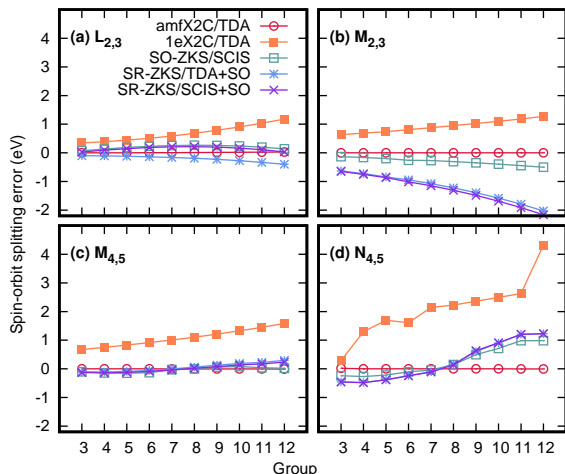


FIG. 4. Error in the X-ray edge splittings for a series of bare, d^0 transition metal cations, computed with different relativistic Hamiltonians and approximations. The splittings are calculated with respect to the spectral features with dominant $p_{3/2} \leftrightarrow d_{5/2}$ and $p_{1/2} \leftrightarrow d_{3/2}$ character.

On average, the errors for the SR-ZKS/TDA+SO and

SR-ZKS/SCIS+SO methods are -0.21 and -0.14 eV for $\Delta L_{2,3}$, -1.22 and -1.30 for $\Delta M_{2,3}$, 0.05 and 0.01 eV for $\Delta M_{4,5}$, and 0.25 and 0.24 eV for $\Delta N_{4,5}$, respectively.

Based on these results, the SR-ZKS/SCIS+SO approach seems to provide the best compromise between cost and accuracy. In order to assess its performance in a more realistic situation, we calculated the $L_{2,3}$, $M_{2,3}$, $M_{4,5}$, and $N_{4,5}$ -edge spectra of several cyanometallates covering different portions of the periodic table (Figure 5).

B. Cyanometallates

Figure 5 shows the X-ray absorption spectra calculated using the state-interaction-based SR-ZKS/SCIS+SO (SR-ZKS) approach versus those calculated using the damped-response (DR) TD-DFT framework paired with the molecular mean-field X2C Hamiltonian (SO-X2C) of Konecny *et al.*⁶² as a reference.

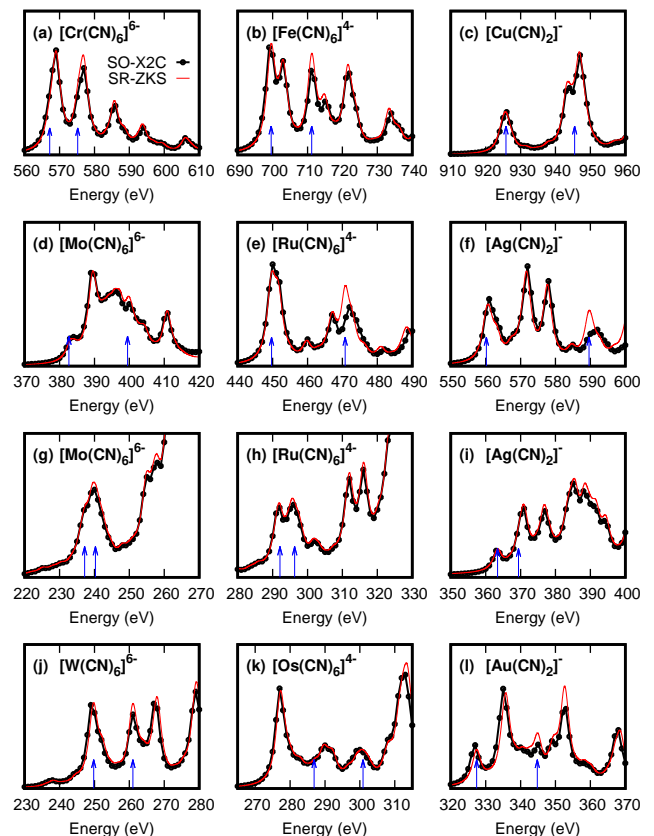


FIG. 5. Soft X-ray absorption spectra of cyanometallates at different edges calculated with the SR-ZKS/SCIS+SO (SR-ZKS) and mmfX2C/DR-TDDFT (SO-X2C) methods. A uniform Lorentzian broadening of 1.5 eV was applied to each spectrum. Spectra are shown for the $L_{2,3}$ (a-c), $M_{2,3}$ (d-f), $M_{4,5}$ (g-i), and $N_{4,5}$ (j-l) edges.

As one can observe, the SR-ZKS/SCIS+SO spectra reproduces the mmfX2C/DR-TDDFT remarkably well,

$\Delta L_{2,3}$	Sc ³⁺	Ti ⁴⁺	V ⁵⁺	Cr ⁶⁺	Mn ⁷⁺	Fe ⁸⁺	Co ⁹⁺	Ni ¹⁰⁺	Cu ¹¹⁺	Zn ¹²⁺	MSD	RMSD
DKS/TDA	4.48	5.66	7.01	8.52	10.21	12.10	14.22	16.60	19.26	22.25		
amfX2C/TDA	4.48	5.67	7.01	8.53	10.22	12.12	14.24	16.62	19.29	22.28	0.01	0.00
1eX2C/TDA	4.82	6.05	7.45	9.03	10.80	12.79	15.01	17.50	20.30	23.43	0.69	0.23
SO-ZKS/SCIS	4.55	5.80	7.20	8.75	10.47	12.37	14.48	16.84	19.46	22.39	0.20	0.07
SR-ZKS/TDA+SO	4.38	5.56	6.89	8.38	10.05	11.91	14.00	16.32	18.93	21.85	-0.21	0.07
SR-ZKS/SCIS+SO	4.51	5.76	7.16	8.71	10.42	12.32	14.43	16.77	19.37	22.28	0.14	0.05
$\Delta M_{2,3}$	Y ³⁺	Zr ⁴⁺	Nb ⁵⁺	Mo ⁶⁺	Tc ⁷⁺	Ru ⁸⁺	Rh ⁹⁺	Pd ¹⁰⁺	Ag ¹¹⁺	Cd ¹²⁺	MSD	RMSD
DKS/TDA	11.83	13.42	15.21	17.12	19.27	21.61	24.18	26.98	30.03	33.34		
amfX2C/TDA	11.83	13.42	15.21	17.12	19.27	21.61	24.18	26.98	30.03	33.34	0.00	0.00
1eX2C/TDA	12.46	14.11	15.94	17.93	20.14	22.56	25.20	28.08	31.21	34.61	0.93	0.30
SO-ZKS/SCIS	11.69	13.26	15.01	16.86	19.00	21.31	23.83	26.59	29.58	32.84	-0.30	0.10
SR-ZKS/TDA+SO	11.20	12.70	14.37	16.18	18.19	20.39	22.79	25.40	28.24	31.31	-1.22	0.41
SR-ZKS/SCIS+SO	11.18	12.67	14.34	16.11	18.12	20.31	22.70	25.30	28.12	31.18	-1.30	0.44
$\Delta M_{4,5}$	Y ³⁺	Zr ⁴⁺	Nb ⁵⁺	Mo ⁶⁺	Tc ⁷⁺	Ru ⁸⁺	Rh ⁹⁺	Pd ¹⁰⁺	Ag ¹¹⁺	Cd ¹²⁺	MSD	RMSD
DKS/TDA	1.90	2.12	2.34	2.56	2.77	3.00	3.25	3.55	3.85	4.18		
amfX2C/TDA	1.90	2.12	2.34	2.56	2.77	3.00	3.25	3.54	3.84	4.18	-0.00	0.00
1eX2C/TDA	2.57	2.87	3.17	3.47	3.78	4.10	4.46	4.88	5.30	5.76	1.09	0.36
SO-ZKS/SCIS	1.80	1.98	2.19	2.42	2.74	3.00	3.31	3.63	3.89	4.20	-0.04	0.03
SR-ZKS/TDA+SO	1.79	2.01	2.25	2.50	2.77	3.06	3.37	3.73	4.07	4.48	0.05	0.05
SR-ZKS/SCIS+SO	1.77	1.99	2.22	2.47	2.73	3.02	3.33	3.69	4.02	4.41	0.01	0.04
$\Delta N_{4,5}$	Lu ³⁺	Hf ⁴⁺	Ta ⁵⁺	W ⁶⁺	Re ⁷⁺	Os ⁸⁺	Ir ⁹⁺	Pt ¹⁰⁺	Au ¹¹⁺	Hg ¹²⁺	MSD	RMSD
DKS/TDA	9.00	9.35	9.65	9.89	10.06	10.23	10.34	10.47	10.65	11.11		
amfX2C/TDA	9.02	9.35	9.65	9.89	10.06	10.23	10.34	10.47	10.64	11.11	0.00	0.00
1eX2C/TDA	9.28	10.64	11.35	11.50	12.21	12.46	12.70	12.96	13.28	15.43	2.11	0.74
SO-ZKS/SCIS	8.76	9.08	9.44	9.78	10.02	10.38	10.83	11.18	11.63	12.09	0.24	0.17
SR-ZKS/TDA+SO	8.54	8.87	9.28	9.66	9.96	10.40	10.94	11.37	11.85	12.34	0.25	0.22
SR-ZKS/SCIS+SO	8.54	8.87	9.27	9.65	9.95	10.37	10.97	11.38	11.85	12.33	0.24	0.22

TABLE III. SO splittings, mean signed deviation (MSD), and root mean squared deviation (RMSD) in the X-ray edge for a series of bare, d^0 transition metal cations, computed with different relativistic Hamiltonians and approximations. The splittings are calculated with respect to the spectral features with dominant $p_{3/2} \leftrightarrow d_{5/2}$ and $p_{1/2} \leftrightarrow d_{3/2}$ character.

given the approximations made in the former. Small discrepancies are visible in the $M_{2,3}$ -edge spectra of $[\text{Ru}(\text{CN})_6]^{4-}$ (Figure 5e) and $[\text{Ag}(\text{CN})_2]^-$ (Figure 5f). These discrepancies are a direct result of the consistent underestimation of the $\Delta M_{2,3}$ splittings by the SR-ZKS approach, causing the M_2 and M_3 features to overlap more than they should. For instance, the feature near 470 eV in the $[\text{Ru}(\text{CN})_6]^{4-}$ is in fact two peaks corresponding to excitations of dominant $3p_{3/2} \rightarrow 5d$ and $3p_{1/2} \rightarrow 4d$ characters. In the SO-X2C calculation, these features have a slightly larger energy separation leading to a broader, lower intensity feature, whereas in SR-ZKS, the features appear as a single peak of higher intensity.

A similar observation can be made for near 590 eV for $[\text{Ag}(\text{CN})_2]^-$.

The peaks chosen to measure the SO splitting in the X-ray edges are marked as blue arrows in Figure 5. Here we chose the lowest-energy features with dominant $p_{3/2} \rightarrow d$ and $p_{1/2} \rightarrow d$ character as a reference for the $X_{2,3}$ -edge spectra, and the lowest-energy features with dominant $d_{5/2} \rightarrow p$ and $d_{3/2} \rightarrow p$ character as a reference for the $X_{4,5}$ -edge spectra, where X correspond to the L, M, or N edges.

An important observation to be made is that the strongest features in the spectra do not always coincide with the metal-centered $p \leftrightarrow d$ features. A clear illustra-

tion of this can be seen in the case of $[\text{Cr}(\text{CN})_6]^{6-}$, where the metal centered $2p_{3/2} \rightarrow 4d$ (e_g) appears around 567 eV next to a stronger metal-to-ligand $2p_{3/2} \rightarrow \pi_L^*$ (t_{2g}) feature at 569 eV. For $[\text{Fe}(\text{CN})_6]^{4-}$, on the other hand, these features are better separated at 700 and 703 eV, respectively, with the metal-centered absorption having slightly higher intensity. By further inspecting the orbital contributions to each excitation, one can conclude that the larger overlap between these features observed in the Cr L-edge leads to mixing between the two states and consequently to an intensity transfer from the $2p_{3/2} \rightarrow 4d$ (e_g) to the $2p_{3/2} \rightarrow \pi_L^*$ (t_{2g}) features.

Furthermore, one can observe that the Mo $M_{2,3}$ -edge in $[\text{Mo}(\text{CN})_6]^{6-}$ and Os $N_{4,5}$ -edge in $[\text{Os}(\text{CN})_6]^{4-}$ appear at the same energy window as the ligand K-edge, which dominate the spectra. This is clearly obvious in the Os N-edge case, where the simulated spectrum closely resembles the C K-edge spectrum expected for unsaturated organic molecules⁶⁴. These observations should be taken into consideration when designing an experiment to probe these edges due to overlapping energies.

VI. CONCLUSIONS

We explored the applicability of a linear-response treatment for a ZKS Hamiltonian, based on the relativistic model potential approach of van Wüllen^{41,42}, to simulate soft X-ray near-edge absorption spectra in closed-shell transition metal systems. Our study demonstrated that spin-orbit coupling effects can be efficiently incorporated using the state-interaction approach, which combines singlet and triplet CIS-like states from scalar-relativistic calculations. We examined two approximations—one including the exchange-correlation contribution in the response equations and one without it. A key advantage of the model potential approach is its compatibility with standard, contracted basis sets, thereby avoiding the high computational costs associated with uncontracted basis sets in fully relativistic calculations.

Our results show that this method accurately reproduces spin-orbit splittings across the periodic table. For bare transition metal cations, the predicted X-ray edge splittings align well with those from 4-component DKS methods. Additionally, for a series of cyanometallates, the state-interaction ZKS approach yields near-edge X-ray absorption spectra that closely agree with results from state-of-the-art X2C methods, all while significantly reducing computational cost.

While not intended to replace more rigorous methods, this quasi-relativistic approach offers a practical alternative for efficiently computing core-level spectra in large, closed-shell transition metal complexes. It is particularly advantageous in cases where full relativistic calculations become computationally prohibitive. Moreover, this method is especially useful for capturing a large number of excited states, making it well-suited for applications such as resonant inelastic X-ray scattering simula-

tions.

Acknowledgments

This work was supported by the National Science Foundation under the CAREER grant No. CHE-2337902 (S. P. M. A. D. and D. R. N.). N. G. acknowledges support by the U.S. Department of Energy, Office of Science, Office of Basic Energy Sciences through the Condensed Phase and Interfacial Molecular Science Program of the Division of Chemical Sciences, Geosciences, and Biosciences of the U.S. Department of Energy (DOE) at Pacific Northwest National Laboratory under FWP 80818. This research benefited from computational resources provided by the University of Memphis High-Performance Computing Facility.

- ¹W. Ackermann, G. Asova, V. Ayvazyan, A. Azima, N. Baboi, J. Bähr, V. Balandin, B. Beutner, A. Brandt, and A. Bolzmann, “Operation of a free-electron laser from the extreme ultraviolet to the water window,” *Nat. Photonics* (2007), 10.1038/nphoton.2007.76i.
- ²P. Emma, R. Akre, J. Arthur, R. Bionta, C. Bostedt, J. Bozek, A. Brachmann, P. Bucksbaum, R. Coffee, F. J. Decker, Y. Ding, D. Dowell, S. Edstrom, A. Fisher, J. Frisch, S. Gilevich, J. Hastings, G. Hays, P. Hering, Z. Huang, R. Iversen, H. Loos, M. Messerschmidt, A. Miahnahri, S. Moeller, H. D. Nuhn, G. Pile, D. Ratner, J. Rzepiela, D. Schultz, T. Smith, P. Stefan, H. Tompkins, J. Turner, J. Welch, W. White, J. Wu, G. Yocky, and J. Galayda, “First lasing and operation of an ångstrom-wavelength free-electron laser,” *Nat. Photonics* **4**, 641–647 (2010).
- ³N. Huang, H. Deng, B. Liu, D. Wang, and Z. Zhao, “Features and futures of x-ray free-electron lasers,” *The Innovation* **2**, 100097 (2021).
- ⁴O. Alexander, F. Egun, L. Rego, A. M. Gutierrez, D. Garratt, G. A. Cárdenas, J. J. Nogueira, J. P. Lee, K. Zhao, R.-P. Wang, D. Ayuso, J. C. T. Barnard, S. Beauvarlet, P. H. Bucksbaum, D. Cesar, R. Coffee, J. Duris, L. J. Frasinski, N. Huse, K. M. Kowalczyk, K. A. Larsen, M. Matthews, S. Mukamel, J. T. O’Neal, T. Penfold, E. Thierstein, J. W. G. Tisch, J. R. Turner, J. Vogwell, T. Driver, N. Berrah, M.-F. Lin, G. L. Dakovski, S. P. Moeller, J. P. Cryan, A. Marinelli, A. Picón, and J. P. Marangos, “Attosecond impulsive stimulated x-ray raman scattering in liquid water,” *Sci. Adv.* **10**, eadp0841 (2024), <https://www.science.org/doi/pdf/10.1126/sciadv.adp0841>.
- ⁵S. Li, L. Lu, S. Bhattacharyya, C. Pearce, K. Li, E. T. Nienhuis, G. Doumy, R. D. Schaller, S. Moeller, M.-f. Lin, G. Dakovski, D. J. Hoffman, D. Garratt, K. A. Larsen, J. D. Koralek, C. Y. Hampton, D. Cesar, J. Duris, Z. Zhang, N. Sudar, J. P. Cryan, A. Marinelli, X. Li, L. Inhester, R. Santra, and L. Young, “Attosecond-pump attosecond-probe x-ray spectroscopy of liquid water,” *Sci. Adv.* , 1118 (2024).
- ⁶G. Lin, C. O. Barnes, S. Weiss, B. Dutagaci, C. Qiu, M. Feig, J. Song, A. Lyubimov, A. E. Cohen, C. D. Kaplan, and G. Calero, “Structural basis of transcription: Rna polymerase ii substrate binding and metal coordination using a free-electron laser,” *Proc. Natl. Acad. Sci.* **121**, e2318527121 (2024).
- ⁷T. Driver, M. Mountney, J. Wang, L. Ortmann, A. Al-Haddad, N. Berrah, C. Bostedt, E. G. Champenois, L. F. DiMauro, J. Duris, D. Garratt, J. M. Glowina, Z. Guo, D. Haxton, E. Isele, I. Ivanov, J. Ji, A. Kamalov, S. Li, M. F. Lin, J. P. Marangos, R. Obaid, J. T. O’Neal, P. Rosenberger, N. H. Shivaram, A. L. Wang, P. Walter, T. J. Wolf, H. J. Wörner, Z. Zhang, P. H. Bucksbaum, M. F. Kling, A. S. Landsman, R. R. Lucchese, A. Emmanouilidou, A. Marinelli, and J. P. Cryan, “Attosecond delays in X-ray molecular ionization,” *Nature* **632**, 762–767 (2024).
- ⁸Z. Guo, T. Driver, S. Beauvarlet, D. Cesar, J. Duris, P. L. Franz,

- O. Alexander, D. Bohler, C. Bostedt, V. Averbukh, X. Cheng, L. F. DiMauro, G. Doumy, R. Forbes, O. Gessner, J. M. Glowina, E. Isele, A. Kamalov, K. A. Larsen, S. Li, X. Li, M. F. Lin, G. A. McCracken, R. Obaid, J. T. O’Neal, R. R. Robles, D. Rolles, M. Ruberti, A. Rudenko, D. S. Slaughter, N. S. Sudar, E. Thierstein, D. Tuthill, K. Ueda, E. Wang, A. L. Wang, J. Wang, T. Weber, T. J. Wolf, L. Young, Z. Zhang, P. H. Bucksbaum, J. P. Marangos, M. F. Kling, Z. Huang, P. Walter, L. Inhester, N. Berrah, J. P. Cryan, and A. Marinelli, “Experimental demonstration of attosecond pump–probe spectroscopy with an X-ray free-electron laser,” *Nat. Photonics* **18**, 691–697 (2024).
- ⁹C. D. Hutchison, J. M. Baxter, A. Fitzpatrick, G. Dorlhiac, A. Fadini, S. Perrett, K. Maghlaoui, S. B. Lefevre, V. Cordon-Preciado, J. L. Ferreira, V. U. Chukhutsina, D. Garratt, J. Barnard, G. Galinis, F. Glencross, R. M. Morgan, S. Stockton, B. Taylor, L. Yuan, M. G. Romei, C. Y. Lin, J. P. Marangos, M. Schmidt, V. Chatrchyan, T. Buckup, D. Morozov, J. Park, S. Park, I. Eom, M. Kim, D. Jang, H. Choi, H. J. Hyun, G. Park, E. Nango, R. Tanaka, S. Owada, K. Tono, D. P. DePonte, S. Carbajo, M. Seaberg, A. Aquila, S. Boutet, A. Barty, S. Iwata, S. G. Boxer, G. Groenhof, and J. J. van Thor, “Optical control of ultrafast structural dynamics in a fluorescent protein,” *Nat. Chem.* **15**, 1607–1615 (2023).
- ¹⁰A. Bhowmick, R. Hussein, I. Bogacz, P. S. Simon, M. Ibrahim, R. Chatterjee, M. D. Doyle, M. H. Cheah, T. Fransson, P. Chernev, I. S. Kim, H. Makita, M. Dasgupta, C. J. Kaminsky, M. Zhang, J. Gätcke, S. Haupt, I. I. Nangca, S. M. Keable, A. O. Aydin, K. Tono, S. Owada, L. B. Gee, F. D. Fuller, A. Batyuk, R. Alonso-Mori, J. M. Holton, D. W. Palle, N. W. Moriarty, F. Mamedov, P. D. Adams, A. S. Brewster, H. Dobbek, N. K. Sauter, U. Bergmann, A. Zouni, J. Messinger, J. Kern, J. Yano, and V. K. Yachandra, “Structural evidence for intermediates during O₂ formation in photosystem II,” *Nature* **617**, 629–636 (2023).
- ¹¹D. Leshchev, A. J. S. Valentine, P. Kim, A. W. Mills, S. Roy, A. Chakraborty, E. Biasin, K. Haldrup, D. J. Hsu, M. S. Kirschner, D. Rimmerman, M. Chollet, J. M. Glowina, T. B. van Driel, F. N. Castellano, X. Li, and L. X. Chen, “Revealing Excited-State Trajectories on Potential Energy Surfaces with Atomic Resolution in Real Time,” *Angew. Chem. Int. Ed.* **62** (2023), 10.1002/anie.202304615.
- ¹²C. B. Larsen, K. Ledbetter, D. R. Nascimento, E. Biasin, M. Qureshi, S. H. Nowak, D. Sokaras, N. Govind, and A. A. Cordones, “Metal–ligand covalency in the valence excited states of metal dithiolenes revealed by s 1s3p resonant inelastic x-ray scattering,” *J. Am. Chem. Soc.* **146**, 28561–28571 (2024).
- ¹³M. E. Casida and D. Chong, “Recent advances in density functional methods,” *Computational Chemistry: Reviews of Current Trends* (1995).
- ¹⁴M. E. Casida, “Time-dependent density-functional theory for molecules and molecular solids,” *J. Mol. Struct.* **914**, 3–18 (2009).
- ¹⁵X. Li, N. Govind, C. Isborn, A. E. DePrince III, and K. Lopata, “Real-time time-dependent electronic structure theory,” *Chem. Rev.* **120**, 9951–9993 (2020).
- ¹⁶S. I. Bokarev and O. Kühn, “Theoretical x-ray spectroscopy of transition metal compounds,” *Wiley Interdiscip. Rev. Comput. Mol. Sci.* **10**, e1433 (2020).
- ¹⁷D. R. Nascimento and N. Govind, “Computational approaches for xanes, vtc-xes, and rixs using linear-response time-dependent density functional theory based methods,” *Phys. Chem. Chem. Phys.* **24**, 14680–14691 (2022).
- ¹⁸M. Kadek, L. Konecny, B. Gao, M. Repisky, and K. Ruud, “X-ray absorption resonances near l 2, 3-edges from real-time propagation of the dirac–kohn–sham density matrix,” *Phys. Chem. Chem. Phys.* **17**, 22566–22570 (2015).
- ¹⁹L. Ye, H. Wang, Y. Zhang, and W. Liu, “Self-adaptive real-time time-dependent density functional theory for x-ray absorptions,” *J. Chem. Phys.* **157**, 074106 (2022).
- ²⁰L. Konecny, J. Vicha, S. Komorovsky, K. Ruud, and M. Repisky, “Accurate x-ray absorption spectra near l-and m-edges from relativistic four-component damped response time-dependent density functional theory,” *Inorg. Chem.* **61**, 830–846 (2021).
- ²¹T. F. Stetina, J. M. Kasper, and X. Li, “Modeling l2, 3-edge x-ray absorption spectroscopy with linear response exact two-component relativistic time-dependent density functional theory,” *J. Chem. Phys.* **150**, 234103 (2019).
- ²²J. M. Kasper, P. J. Lestrangle, T. F. Stetina, and X. Li, “Modeling l2, 3-edge x-ray absorption spectroscopy with real-time exact two-component relativistic time-dependent density functional theory,” *J. Chem. Theory Comput.* **14**, 1998–2006 (2018).
- ²³M. Stener, G. Fronzoni, and M. d. de Simone, “Time dependent density functional theory of core electrons excitations,” *Chem. Phys. Lett.* **373**, 115–123 (2003).
- ²⁴F. Wang, T. Ziegler, E. van Lenthe, S. van Gisbergen, and E. J. Baerends, “The calculation of excitation energies based on the relativistic two-component zeroth-order regular approximation and time-dependent density-functional with full use of symmetry,” *J. Chem. Phys.* **122**, 204103 (2005).
- ²⁵G. Fronzoni, M. Stener, P. Decleva, F. Wang, T. Ziegler, E. Van Lenthe, and E. Baerends, “Spin-orbit relativistic time dependent density functional theory calculations for the description of core electron excitations: TiCl₄ case study,” *Chem. Phys. Lett.* **416**, 56–63 (2005).
- ²⁶M. Casarin, P. Finetti, A. Vittadini, F. Wang, and T. Ziegler, “Spin-orbit relativistic time-dependent density functional calculations of the metal and ligand pre-edge xas intensities of organotitanium complexes: TiCl₄, ti (η^5 -c₅h₅) cl₃, and ti (η^5 -c₅h₅) 2cl₂,” *J. Phys. Chem. A* **111**, 5270–5279 (2007).
- ²⁷G. Fronzoni, R. De Francesco, and M. Stener, “L2, 3 edge photoabsorption spectra of bulk v2o5: a two components relativistic time dependent density functional theory description with finite cluster model,” *J. Chem. Phys.* **137**, 224308 (2012).
- ²⁸W. Hua, G. Tian, G. Fronzoni, X. Li, M. Stener, and Y. Luo, “Fe l-edge x-ray absorption spectra of fe (ii) polypyridyl spin crossover complexes from time-dependent density functional theory,” *J. Phys. Chem. A* **117**, 14075–14085 (2013).
- ²⁹H. Stoll, B. Metz, and M. Dolg, “Relativistic energy-consistent pseudopotentials—recent developments,” *J. Comput. Chem.* **23**, 767–778 (2002).
- ³⁰K. Hirao and Y. Ishikawa, *Recent Advances in Relativistic Molecular Theory* (World Scientific, 2004).
- ³¹M. Dolg and X. Cao, “Relativistic pseudopotentials: their development and scope of applications,” *Chem. Rev.* **112**, 403–480 (2012).
- ³²N. S. Mosyagin, A. V. Zaitsevskii, L. V. Skripnikov, and A. V. Titov, “Generalized relativistic effective core potentials for actinides,” *Int. J. Quantum Chem.* **116**, 301–315 (2016).
- ³³J. Liu and L. Cheng, “Relativistic coupled-cluster and equation-of-motion coupled-cluster methods,” *Wiley Interdiscip. Rev. Comput. Mol. Sci.* **11**, e1536 (2021).
- ³⁴R. M. Jay, K. Kunnus, P. Wernet, and K. J. Gaffney, “Capturing atom-specific electronic structural dynamics of transition-metal complexes with ultrafast soft x-ray spectroscopy,” *Annu. Rev. Phys. Chem.* **73**, 187–208 (2022).
- ³⁵S. Lee, H. Zhai, and G. K.-L. Chan, “An ab initio correction vector restricted active space approach to the l-edge xas and 2p3d rixs spectra of transition metal complexes,” *J. Chem. Theory Comput.* **19**, 7753–7763 (2023).
- ³⁶A. W. Hahn, B. E. Van Kuiken, V. G. Chilkuri, N. Levin, E. Bill, T. Weyhermüller, A. Nicolaou, J. Miyawaki, Y. Harada, and S. DeBeer, “Probing the valence electronic structure of low-spin ferrous and ferric complexes using 2p3d resonant inelastic x-ray scattering (rixs),” *Inorg. Chem.* **57**, 9515–9530 (2018).
- ³⁷D. R. Nascimento, E. Biasin, B. I. Poulter, M. Khalil, D. Sokaras, and N. Govind, “Resonant inelastic x-ray scattering calculations of transition metal complexes within a simplified time-dependent density functional theory framework,” *J. Chem. Theory Comput.* **17**, 3031–3038 (2021).
- ³⁸C. Van Stappen, B. E. Van Kuiken, M. Mörtel, K. O. Ruot-salainen, D. Maganas, M. M. Khusniyarov, and S. DeBeer,

- “Correlating valence and 2p3d rixs spectroscopies: A ligand-field study of spin-crossover iron (ii),” *Inorg. Chem.* **63**, 7386–7400 (2024).
- ³⁹E. Biasin, D. R. Nascimento, B. I. Poulter, B. Abraham, K. Kunnus, A. T. Garcia-Esparza, S. H. Nowak, T. Kroll, R. W. Schoenlein, R. Alonso-Mori, M. Khalil, N. Govind, and D. Sokaras, “Revealing the bonding of solvated ru complexes with valence-to-core resonant inelastic x-ray scattering,” *Chem. Sci.*, DOI:10.1039/D0SC06227H (2021).
- ⁴⁰B. I. Poulter, E. Biasin, S. H. Nowak, T. Kroll, R. Alonso-Mori, R. W. Schoenlein, N. Govind, D. Sokaras, and M. Khalil, “Uncovering the 3d and 4d electronic interactions in solvated ru complexes with 2p3d resonant inelastic x-ray scattering,” *Inorganic Chemistry* **62**, 9904–9911 (2023).
- ⁴¹C. van Wüllen, “Molecular density functional calculations in the regular relativistic approximation: Method, application to coinage metal diatomics, hydrides, fluorides and chlorides, and comparison with first-order relativistic calculations,” *J. Chem. Phys.* **109**, 392–399 (1998).
- ⁴²C. Van Wüllen and C. Michauk, “Accurate and efficient treatment of two-electron contributions in quasirelativistic high-order douglas-kroll density-functional calculations,” *The Journal of chemical physics* **123** (2005).
- ⁴³J. Van Lenthe, S. Faas, and J. Snijders, “Gradients in the ab initio scalar zeroth-order regular approximation (zora) approach,” *Chemical Physics Letters* **328**, 107–112 (2000).
- ⁴⁴S. Faas, J. Van Lenthe, A. Hennum, and J. Snijders, “An ab initio two-component relativistic method including spin-orbit coupling using the regular approximation,” *The Journal of Chemical Physics* **113**, 4052–4059 (2000).
- ⁴⁵J. Van Lenthe and J. Van Lingen, “Note on the calculation of analytical Hessians in the zeroth-order regular approximation (zora),” *International journal of quantum chemistry* **106**, 2525–2528 (2006).
- ⁴⁶P. Nichols, N. Govind, E. J. Bylaska, and W. A. de Jong, “Gaussian Basis Set and Planewave Relativistic Spin-Orbit Methods in NWChem,” *J. Chem. Theory Comput.* **5**, 491–499 (2009).
- ⁴⁷E. van Lenthe, E. J. Baerends, and J. G. Snijders, “Relativistic total energy using regular approximations,” *J. Chem. Phys.* **101**, 9783–9792 (1994), <https://doi.org/10.1063/1.467943>.
- ⁴⁸S. Pak and D. R. Nascimento, “The role of the coupling matrix elements in time-dependent density functional theory on the simulation of core-level spectra of transition metal complexes,” *Electron. Struct.* **6**, 015014 (2024).
- ⁴⁹P.-Å. Malmqvist and B. O. Roos, “The casscf state interaction method,” *Chem. Phys. Lett.* **155**, 189–194 (1989).
- ⁵⁰M. Valiev, E. Bylaska, N. Govind, K. Kowalski, T. Straatsma, H. V. Dam, D. Wang, J. Nieplocha, E. Apra, T. Windus, and W. de Jong, “Nwchem: A comprehensive and scalable open-source solution for large scale molecular simulations,” *Comput. Phys. Commun.* **181**, 1477 – 1489 (2010).
- ⁵¹E. Aprà, E. J. Bylaska, W. A. de Jong, N. Govind, K. Kowalski, T. P. Straatsma, M. Valiev, H. J. J. van Dam, Y. Alexeev, J. Anchell, V. Anisimov, F. W. Aquino, R. Atta-Fynn, J. Autschbach, N. P. Bauman, J. C. Becca, D. E. Bernholdt, K. Bhaskaran-Nair, S. Bogatko, P. Borowski, J. Boschen, J. Brabec, A. Bruner, E. Cauët, Y. Chen, G. N. Chuev, C. J. Cramer, J. Daily, M. J. O. Deegan, T. H. Dunning, M. Dupuis, K. G. Dyall, G. I. Fann, S. A. Fischer, A. Fonari, H. Früchtl, L. Gagliardi, J. Garza, N. Gawande, S. Ghosh, K. Glaesemann, A. W. Götz, J. Hammond, V. Helms, E. D. Hermes, K. Hirao, S. Hirata, M. Jacquelin, L. Jensen, B. G. Johnson, H. Jónsson, R. A. Kendall, M. Klemm, R. Kobayashi, V. Konkov, S. Krishnamoorthy, M. Krishnan, Z. Lin, R. D. Lins, R. J. Littlefield, A. J. Logsdail, K. Lopata, W. Ma, A. V. Marenich, J. Martin del Campo, D. Mejia-Rodriguez, J. E. Moore, J. M. Mullin, T. Nakajima, D. R. Nascimento, J. A. Nichols, P. J. Nichols, J. Nieplocha, A. Otero-de-la Roza, B. Palmer, A. Panyala, T. Pirojsirikul, B. Peng, R. Peverati, J. Pittner, L. Pollack, R. M. Richard, P. Sadayappan, G. C. Schatz, W. A. Shelton, D. W. Silverstein, D. M. A. Smith, T. A. Soares, D. Song, M. Swart, H. L. Taylor, G. S. Thomas, V. Tipparaju, D. G. Truhlar, K. Tsemekhman, T. Van Voorhis, Á. Vázquez-Mayagoitia, P. Verma, O. Villa, A. Vishnu, K. D. Vogiatzis, D. Wang, J. H. Weare, M. J. Williamson, T. L. Windus, K. Woliński, A. T. Wong, Q. Wu, C. Yang, Q. Yu, M. Zacharias, Z. Zhang, Y. Zhao, and R. J. Harrison, “Nwchem: Past, present, and future,” *J. Chem. Phys.* **152**, 184102 (2020), <https://doi.org/10.1063/5.0004997>.
- ⁵²J. P. Perdew, M. Ernzerhof, and K. Burke, “Rationale for mixing exact exchange with density functional approximations,” *J. Chem. Phys.* **105**, 9982–9985 (1996).
- ⁵³C. Adamo and V. Barone, “Toward reliable density functional methods without adjustable parameters: The pbe0 model,” *J. Chem. Phys.* **110**, 6158–6170 (1999).
- ⁵⁴R. Ditchfield, W. J. Hehre, and J. A. Pople, “Self-consistent molecular-orbital methods. ix. an extended gaussian-type basis for molecular-orbital studies of organic molecules,” *J. Chem. Phys.* **54**, 724–728 (1971).
- ⁵⁵W. J. Hehre, R. Ditchfield, and J. A. Pople, “Self-consistent molecular orbital methods. xii. further extensions of gaussian-type basis sets for use in molecular orbital studies of organic molecules,” *J. Chem. Phys.* **56**, 2257–2261 (1972).
- ⁵⁶P. C. Hariharan and J. A. Pople, “The influence of polarization functions on molecular orbital hydrogenation energies,” *Theor. Chim. Acta* **28**, 213–222 (1973).
- ⁵⁷T. Noro, M. Sekiya, and T. Koga, “Segmented contracted basis sets for atoms h through xe: Sapporo-(dk)-nzp sets (n= d, t, q),” *Theor. Chem. Acc.* **131**, 1124 (2012).
- ⁵⁸K. G. Dyall, “Relativistic double-zeta, triple-zeta, and quadruple-zeta basis sets for the 4d elements y–cd,” *Theor. Chem. Acc.* **117**, 483–489 (2007).
- ⁵⁹K. G. Dyall, “Dyall dz, tz, and qz basis sets for relativistic electronic structure on Zenodo (2023).
- ⁶⁰Q. Sun, T. C. Berkelbach, N. S. Blunt, G. H. Booth, S. Guo, Z. Li, J. Liu, J. D. McClain, E. R. Sayfutyarova, S. Sharma, S. Wouters, and G. K.-L. Chan, “Pyscf: the python-based simulations of chemistry framework,” *Wiley Interdiscip. Rev. Comput. Mol. Sci.* **8**, e1340 (2018), <https://wires.onlinelibrary.wiley.com/doi/pdf/10.1002/wcms.1340>.
- ⁶¹M. Repisky, S. Komorovsky, M. Kadek, L. Konecny, U. Ekström, E. Malkin, M. Kaupp, K. Ruud, O. L. Malkina, and V. G. Malkin, “Respect: Relativistic spectroscopy dft program package,” *J. Chem. Phys.* **152** (2020).
- ⁶²L. Konecny, S. Komorovsky, J. Vicha, K. Ruud, and M. Repisky, “Exact two-component tddft with simple two-electron picture-change corrections: X-ray absorption spectra near l-and m-edges of four-component quality at two-component cost,” *J. Phys. Chem. A* **127**, 1360–1376 (2023).
- ⁶³J. Ehrman, E. Martinez-Baez, A. J. Jenkins, and X. Li, “Improving one-electron exact-two-component relativistic methods with the dirac-coulomb-breit-parameterized effective spin-orbit coupling,” *J. Chem. Theory Comput.* **19**, 5785–5790 (2023).
- ⁶⁴D. R. Nascimento and A. E. DePrince III, “Simulation of near-edge x-ray absorption fine structure with time-dependent equation-of-motion coupled-cluster theory,” *J. Phys. Chem. Lett.* **8**, 2951–2957 (2017).